Quasiparticle states near surfaces of high-T_c superconductors based on the extended t-J model

Y. Tanuma
Graduate School of Science and Technology, Niigata University, Ikarashi, Niigata 950-2181, Japan

Y. Tanaka
Department of Applied Physics, Nagoya University, Nagoya 464-8063, Japan

M. Ogata
Department of Basic Science, Graduate School of Arts and Sciences, University of Tokyo, 3-8-1 Komaba, Meguro-ku, Tokyo 153-8902, Japan

S. Kashiwaya
Electrotechnical Laboratory, Tsukuba, Ibaraki 305-8568, Japan

(Received 22 March 1999)

Quasiparticle properties near surfaces of d-wave superconductors are numerically studied based on the extended t-J model with Gutzwiller approximation. In order to simulate detailed profiles of the local density of states, the amplitudes of the transfer integrals are chosen so as to reproduce the Fermi surfaces of high-T_c superconductors. It is shown that the spatial dependence of the local density of states is sensitive to the geometry of the surface, the shape of the Fermi surface, and the doping rate δ. In particular, clear δ dependences are obtained in spectral features, i.e., zero-energy peaks and their splitting due to the inducement of an s-wave component which breaks time-reversal symmetry. The present results suggest that the microscopic parameters of actual materials can be extracted from a detailed analysis of scanning tunneling spectroscopy data. [S0163-1829(99)05337-0]

I. INTRODUCTION

Since the discovery of high-T_c superconductors, there has been much evidence from both experimental and theoretical studies that the symmetry of pair potentials in high-T_c superconductors is $d_{x^2-y^2}$ wave.[1] The essential difference of $d_{x^2-y^2}$-wave symmetry from conventional s-wave symmetry is the existence of an internal phase of the pair potential, as well as its amplitude variation in k space. The internal phase in actual high-T_c superconductors has been detected as a phase shift in the dc Josephson effect.[2–7] Moreover, recent theoretical and experimental studies have clarified that the internal phase causes a drastic interference effect in quasiparticle states near surfaces and interfaces. At a specularly reflecting (110) surface of a $d_{x^2-y^2}$-wave superconductor, a zero-energy state (ZES) is induced due to the sign change of the effective pair potential.[8] The formation of a ZES results in a peak in the surface density of states at zero energy[9–12] and manifests itself as a so-called zero-bias conductance peak (ZBCP) observed in scanning tunneling spectroscopy (STS).[9,13–24] However, it is also clarified that the ZBCP is strongly influenced by the microscopic geometry and by the quality of surface.[25]

On the other hand, there is the possibility that an order parameter with a different symmetry coexists with the $d_{x^2-y^2}$ wave near the surface where the $d_{x^2-y^2}$-wave amplitude is suppressed. Actually, quasiclassical theory[11,26] shows that the induced subdominant pair potential breaks time-reversal symmetry. Recent tunneling experiments show that the ZBCP splits into two peaks even in the absence of an applied magnetic field,[20,27] which is consistent with the theory.

In spite of a qualitative agreement between theories and experiments, previous theories[11,26] have not taken into account two important points peculiar to high-T_c materials: (i) a short coherence length and (ii) strong electron correlation. Moreover, these theories assume the existence of an s-wave attractive interaction the origin of which is not clear for actual high-T_c superconductors. Thus, in this paper, we study the local density of states (LDOS) near surfaces using the two-dimensional (2D) t-J model, which has the above important features.

The t-J model[28] is one of promising models which explains low-energy excitations in high-T_c superconductors. Although an analytic solution of this model has not been obtained, phase diagrams as a function of doping rate δ and a superexchange interaction J are numerically studied at $T=0$ for one dimension[29] and two dimension.[30–33] Especially, in the 2D t-J model, the obtained phase diagram as a function of doping is consistent with actual high-T_c superconductors. Although there have been presented a lot of works on this model,[32] only several studies have been devoted to the quasiparticle properties in nonuniform systems, e.g., cases with a vortex,[34] impurities,[35] and surfaces.[36–39] In our previous paper,[36] we have shown that the ZBCP on a (110) surface splits due to the broken time-reversal symmetry in the realistic t-J model. Moreover, it is clarified that the splitting is enhanced as the doping rate δ and the magnitude of the superexchange are increased, and that the LDOS is sensitive to microscopic structures near the surface.

In this paper, we extend our previous study to investigate the material dependence and doping dependence. To reproduce the shape of the Fermi surface observed experimentally,

we include the transfer integrals for next-nearest (t') and the third-nearest neighbors (t'') in the same way introduced by Tanamoto *et al.*[41–43] The Gutzwiller approximation has been applied to treat the constraint in the extended t-J model.[40] The reliability of this approximation has been established through comparison between the variational energies of the bulk states in the t-J model and those obtained in the variational Monte Carlo method.[33] The spatial dependence of the pair potential is determined self-consistently as in our previous works.[34–36]

The organization of this paper is as follows. In Sec. II, the formulation to calculate the spatial dependence of the pair potential, Fermi surfaces, and the LDOS is presented. In Sec. III, the results of the numerical calculation for various surface geometries are discussed in detail. Section IV is devoted to a summary and future problems.

II.. FORMULATION

The t-J model is written as[28]

$$\mathcal{H}=-\sum_{\mathbf{i},\mathbf{j},\sigma} t_{\mathbf{ij}}(\tilde{c}^{\dagger}_{\mathbf{i}\sigma}\tilde{c}_{\mathbf{j}\sigma}+\mathrm{H.c.})+J\sum_{\langle\mathbf{i},\mathbf{j}\rangle,\sigma}\mathbf{S_i}\cdot\mathbf{S_j}-\mu\sum_{\mathbf{i},\sigma}c^{\dagger}_{\mathbf{i}\sigma}c_{\mathbf{i}\sigma}, \tag{1}$$

where $\tilde{c}_{\mathbf{i}\sigma}=c_{\mathbf{i}\sigma}(1-n_{\mathbf{i}-\sigma})$, $n_{\mathbf{i}\sigma}=c^{\dagger}_{\mathbf{i}\sigma}c_{\mathbf{i}\sigma}$, and $c_{\mathbf{i}\sigma}$ ($c^{\dagger}_{\mathbf{i}\sigma}$) is the annihilation (creation) operator of an electron with spin σ at site $\mathbf{i}$ in a 2D square lattice. Here $\mathbf{i}=(i_x,j_y)$ and $\mathbf{j}=(j_x,j_y)$ are position coordinates in the lattice, and the summation $\langle\mathbf{i},\mathbf{j}\rangle$ runs over nearest-neighbor pairs. The quantities J, $\mathbf{S_i}$, and μ stand for the superexchange interaction, the spin-1/2 operator, and the chemical potential, respectively. The transfer integrals up to the third-nearest-neighbor sites are included as the first term of Eq. (1). These amplitudes $t_{\mathbf{ij}}$ are chosen as follows:

$$t_{\mathbf{ij}}=\begin{cases} t\ (>0), & \text{nearest neighbors,}\\ t'\ (<0), & \text{next-nearest neighbors,}\\ t''\ (>0), & \text{third-nearest neighbors.}\end{cases} \tag{2}$$

We fix $J/t=0.25$ and study the four cases for $t_{\mathbf{ij}}$ following Tanamoto *et al.*:[41–43] (i) the t-J model ($t'=t''=0$), (ii) LSCO type ($t'/t=-1/6$, $t''/t=0$), (iii) YBCO type ($t'/t=-1/6$, $t''/t=1/5$), and (iv) YBCO (II) type ($t'/t=-1/2$, $t''/t=0$). In the following, we call them (i) t-J, (ii) LSCO, (iii) YBCO, and (iv) YBCO (II).

We employ the Gutzwiller approximation[40] where the effect of the projection is taken into account as statistical weights. The expectation values are estimated as

$$\langle c^{\dagger}_{\mathbf{i}\sigma}c_{\mathbf{j}\sigma}\rangle=g_t\langle c^{\dagger}_{\mathbf{i}\sigma}c_{\mathbf{j}\sigma}\rangle_0,$$

$$\langle\mathbf{S_i}\cdot\mathbf{S_j}\rangle=g_s\langle\mathbf{S_i}\cdot\mathbf{S_j}\rangle_0, \tag{3}$$

where $\langle\cdots\rangle$ and $\langle\cdots\rangle_0$ represent the expectation values in terms of Gutzwiller-type variational wave functions $P_G|\Phi\rangle$ and $|\Phi\rangle$, respectively. Here $P_G=\Pi_{\mathbf{i}}(1-n_{\mathbf{i}\uparrow}n_{\mathbf{i}\downarrow})$ is the Gutzwiller projection operator and $|\Phi\rangle$ is a BCS wave function. The renormalized coefficients are given by[40,33]

$$g_t=\frac{2\delta}{1+\delta},\quad g_s=\frac{4}{(1+\delta)^2}, \tag{4}$$

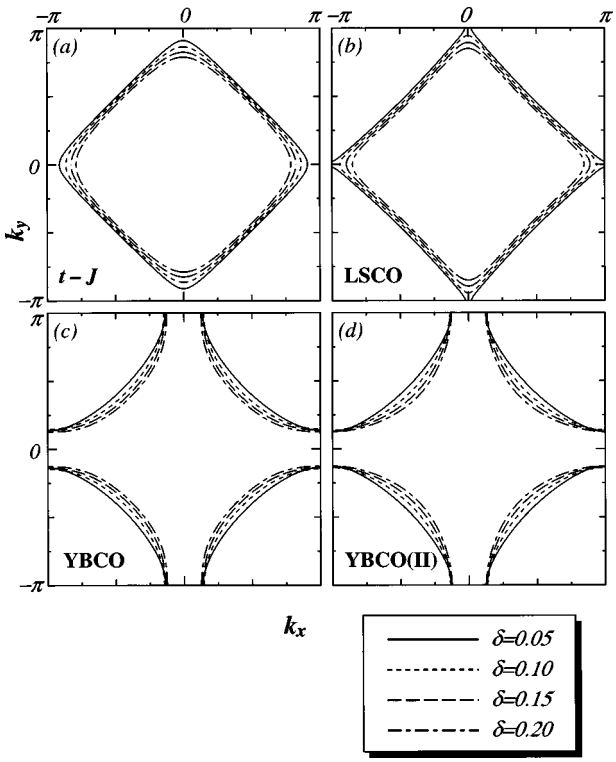

FIG. 1. The Fermi surfaces in the extended t-J model in the Gutzwiller approximation for several doping rates: (a) t-J model ($t'=t''=0$), (b) LSCO type ($t'/t=-1/6$, $t''/t=0$), (c) YBCO type ($t'/t=-1/6$, $t''/t=1/5$), and (d) YBCO (II) type ($t'/t=-1/2$, $t''/t=0$).

with the hole concentration $\delta\,(=1-n)$. Using this approximation, the effective Hamiltonian containing the next- and third-nearest transfer integrals becomes

$$\begin{aligned}\mathcal{H}_{\mathrm{eff}}=&-t_{\mathrm{eff}}\sum_{\langle\mathbf{i},\mathbf{j}\rangle,\sigma}(c^{\dagger}_{\mathbf{i}\sigma}c_{\mathbf{j}\sigma}+\mathrm{H.c.})-t'_{\mathrm{eff}}\sum_{\langle\mathbf{i},\mathbf{j}\rangle',\sigma}(c^{\dagger}_{\mathbf{i}\sigma}c_{\mathbf{j}\sigma}+\mathrm{H.c.})\\&-t''_{\mathrm{eff}}\sum_{\langle\mathbf{i},\mathbf{j}\rangle'',\sigma}(c^{\dagger}_{\mathbf{i}\sigma}c_{\mathbf{j}\sigma}+\mathrm{H.c.})\\&+J_{\mathrm{eff}}\sum_{\langle\mathbf{i},\mathbf{j}\rangle}\mathbf{S_i}\cdot\mathbf{S_j}-\mu\sum_{\mathbf{i},\sigma}c^{\dagger}_{\mathbf{i}\sigma}c_{\mathbf{i}\sigma},\end{aligned} \tag{5}$$

$$t_{\mathrm{eff}}=g_t t,\quad t'_{\mathrm{eff}}=g_t t',\quad t''_{\mathrm{eff}}=g_t t'',\quad J_{\mathrm{eff}}=g_s J, \tag{6}$$

where $\langle\mathbf{i},\mathbf{j}\rangle'$ and $\langle\mathbf{i},\mathbf{j}\rangle''$ represent the summations over the next- and third-nearest neighbor pairs, respectively.

The Fermi surfaces obtained within the Gutzwiller approximation for the four cases of t' and t'' are shown in Fig. 1 as a function of the hole concentration δ. Figure 1(a) shows those in the t-J model with the transfer integral only between nearest-neighbor sites. The amplitudes of t and t' (Refs. 41–43) in Figs. 1(b) and 1(c) are chosen to reproduce the qualitative features of the Fermi surface in LSCO ($=La_{2-x}Sr_xCuO_4$) and YBCO ($=YBa_2Cu_3O_{7-\delta}$) obtained from local density approximation (LDA) band calculations. As shown in Fig. 1(d), the choice of (iv) also gives a quite similar Fermi surface to those in YBCO (II). As regards the reliability of the Gutzwiller approximation, only the total energy of the system is checked to be consistent with that by

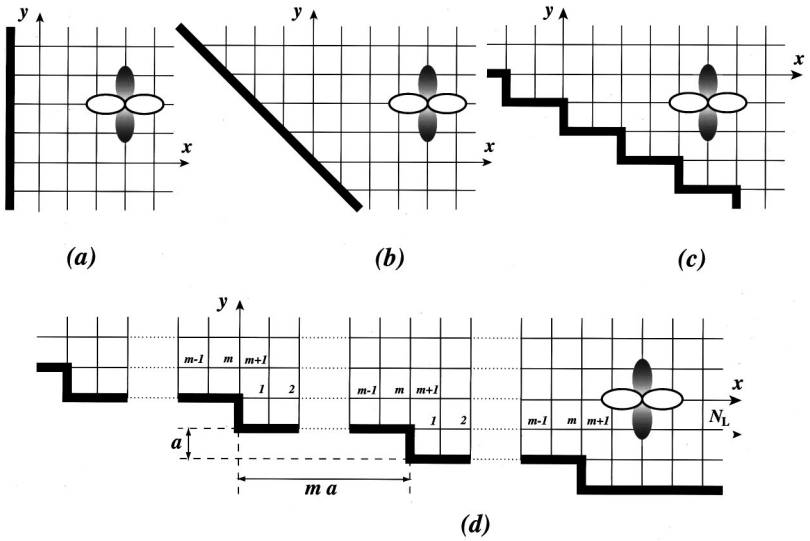

FIG. 2. Schematic illustration corresponding to a $1\times m$ zigzag surface: (a) a flat (100) surface ($m=0$), (b) a flat (110) surface ($m=1$), (c) a 1×2 zigzag surface ($m=2$), and (d) a $1\times m$ zigzag surface.

the variational Monte Carlo method. It is not clear whether this approximation is really available to obtain the quasiparticle spectra in nonuniform systems such as the surface or interface since this approximation does not give an accurate numerical value as regards the magnitude of the superconducting gap and bandwidth. However, the topology of the Fermi surface, which is consistent with photoemission spectroscopy, can be reproduced using this approximation.[41–43] Since our actual interest is restricted to the qualitative difference between the low-energy excitations of the quasiparticle properties near the surface with several materials, it is sufficient to start from the Fermi surface obtained by this approximation.

The geometries of the boundaries used in the following calculation are shown in Fig. 2. The index m in Fig. 2(d) denotes the period of zigzag structures. The case of $m=0$ [$m=1$] corresponds to a flat (100) [(110)] surface as shown in Fig. 2(a) [2(b)]. In the following, we discuss the cases with $m=0$, 1, and 2. In each raw, we have N_L sites.

We perform a mean-field approximation with site-dependent pair potential $\Delta_{\mathbf{ij}}$ and Hartree-Fock parameter $\xi_{\mathbf{ij}\sigma}$,

$$\Delta_{\mathbf{ij}}=\frac{3}{4}J_{\mathrm{eff}}\langle c_{\mathbf{i}\uparrow}c_{\mathbf{j}\downarrow}\rangle,\quad \xi_{\mathbf{ij}\sigma}=\langle c^{\dagger}_{\mathbf{i}\sigma}c_{\mathbf{j}\sigma}\rangle. \tag{7}$$

Here we have assumed $\xi_{\mathbf{ij}\uparrow}=\xi_{\mathbf{ij}\downarrow}=\xi_{\mathbf{ij}}$. For simplicity, $\xi_{\mathbf{ij}}$ and μ are fixed to the values ξ_0 and μ_0 determined in the bulk without boundaries. In this sense, the possibility of an oscillating order parameter found in the bulk t-J model near half-filling[44] is not considered in this paper.

We assume that $\Delta_{\mathbf{ij}}$ is translationally invariant in the tangential direction along the surface. Thus our unit cell is N_L sites in the x direction and a single site in the y direction. To represent $\Delta_{\mathbf{ij}}$, we introduce a new coordinate j along the x direction. The original position coordinate $\mathbf{j}$ is represented as $\mathbf{j}=(-mj_y+j,j_y)$ with $j=1,\ldots,N_L$ and $\Delta_{\mathbf{ij}}$ is rewritten by $\Delta_{ij,x}$ and $\Delta_{ij,y}$. In the y direction, we assume N_y unit cells and the electrons are Fourier transformed as

$$C_{j\uparrow}(k_y)=\sum_{j_y=1}^{N_y}c_{\mathbf{j}\uparrow}e^{-ik_yj_ya},\quad C_{j\downarrow}(-k_y)=\sum_{j_y=1}^{N_y}c_{\mathbf{j}\downarrow}e^{ik_yj_ya}, \tag{8}$$

where a is the lattice constant and

$$-\frac{\pi}{a}<k_y\leqq\frac{\pi}{a},\quad k_y=\frac{2\pi}{N_y}n\quad (n:\ \text{interger}).$$

After the Fourier transformation, the mean-field Hamiltonian becomes

$$\mathcal{H}_{\mathrm{MF}}(m)=\sum_{k_y,i,j}[C^{\dagger}_{i\uparrow}(k_y)C_{i\downarrow}(-k_y)]\times\begin{pmatrix}\hat{H}_{ij}(k_y,m) & \hat{\Delta}_{ij}(k_y,m)\\ \hat{\Delta}^{\dagger}_{ji}(k_y,m) & -\hat{H}_{ji}(-k_y,m)\end{pmatrix}\begin{pmatrix}C_{j\uparrow}(k_y)\\ C^{\dagger}_{j\downarrow}(-k_y)\end{pmatrix}, \tag{9}$$

with

$$\hat{H}_{ij}(k_y,m)=-\sum_{\pm}\Big[\Big(t_{\mathrm{eff}}+\frac{3}{4}J_{\mathrm{eff}}\xi_0\Big)(\delta_{i,j\pm1}+e^{\mp ik_ya}\delta_{i,j\pm m})+t'_{\mathrm{eff}}e^{\mp ik_ya}\delta_{i,j\pm(m+1)}+t'_{\mathrm{eff}}e^{\pm ik_ya}\delta_{i,j\pm(m-1)}+t''_{\mathrm{eff}}(\delta_{i,j\pm2}+e^{\mp2ik_ya}\delta_{i,j\pm2m})\Big]-\mu_0\delta_{i,j}, \tag{10}$$

$$\hat{\Delta}_{ij}(k_y,m)=\sum_{\pm}[\Delta_{ij,x}(m)\delta_{i,j\pm1}+\Delta_{ij,y}(m)e^{\mp ik_ya}\delta_{i,j\pm m}]. \tag{11}$$

The form of the $2N_L\times2N_L$ matrix elements changes according to the number m of zigzag structures shown in Fig. 2. For example, in the case of a flat (110) surface for the t-J model, the elements of the $N_L\times N_L$ small matrix are written as

$$\hat{H}_{ij}(k_y,1)=\begin{pmatrix} -\mu_0 & -\tau_x-\tau_y & 0 & \cdots & \cdots & 0 \\ -\tau_x^*-\tau_y^* & -\mu_0 & -\tau_x-\tau_y & 0 & \cdots & 0 \\ 0 & -\tau_x^*-\tau_y^* & -\mu_0 & -\tau_x-\tau_y & \cdots & 0 \\ \cdots & \cdots & \cdots & \cdots & \cdots & \cdots \\ 0 & \cdots & \cdots & 0 & -\tau_x^*-\tau_x^* & -\mu_0 \end{pmatrix}, \tag{12}$$

with $\tau_x=t_{\rm eff}+3/4J_{\rm eff}\,\xi_0$, $\tau_y=(t_{\rm eff}+3/4J_{\rm eff}\,\xi_0)e^{-ik_ya}$, and

$$\hat{\Delta}_{ij}(k_y,1)=\begin{pmatrix} 0 & \Delta_{12,x}+\Delta_{12,y}e^{-ik_ya} & \cdots & \cdots & 0 \\ \Delta_{21,x}+\Delta_{21,y}e^{ik_ya} & 0 & \Delta_{23,x}+\Delta_{23,y}e^{-ik_ya} & \cdots & 0 \\ 0 & \Delta_{32,x}+\Delta_{32,y}e^{ik_ya} & 0 & \cdots & 0 \\ \cdots & \cdots & \cdots & \cdots & \cdots \\ 0 & \cdots & \cdots & \Delta_{N_L2,x}+\Delta_{N_L2,y}e^{ik_ya} & 0 \end{pmatrix}. \tag{13}$$

Similarly, for a 1×2 zigzag surface, we use

$$\hat{H}_{ij}(k_y,2)=\begin{pmatrix} -\mu_0 & -\tau_x & -\tau_y & 0 & 0 & \cdots & 0 \\ -\tau_x^* & -\mu_0 & -\tau_x & -\tau_y & 0 & \cdots & 0 \\ -\tau_y^* & -\tau_x^* & -\mu_0 & -\tau_x & -\tau_y & \cdots & 0 \\ \cdots & \cdots & \cdots & \cdots & \cdots & \cdots & \cdots \\ 0 & \cdots & \cdots & 0 & -\tau_y^* & -\tau_x^* & -\mu_0 \end{pmatrix}, \tag{14}$$

$$\hat{\Delta}_{ij}(k_y,2)=\begin{pmatrix} 0 & \Delta_{12,x} & \Delta_{13,y}e^{-ik_ya} & 0 & 0 & \cdots & 0 \\ \Delta_{21,x} & 0 & \Delta_{23,x} & \Delta_{24,y}e^{-ik_ya} & 0 & \cdots & 0 \\ \Delta_{31,y}e^{ik_ya} & \Delta_{32,x} & 0 & \Delta_{34,x} & \Delta_{35,y}e^{-ik_ya} & \cdots & 0 \\ \cdots & \cdots & \cdots & \cdots & \cdots & \cdots & \cdots \\ 0 & \cdots & \cdots & 0 & \Delta_{N_LN_L-2,y}e^{-ik_ya} & \Delta_{N_LN_L-1,x} & 0 \end{pmatrix}. \tag{15}$$

We choose the total site number $N_L=401$ and $N_y=80$ to calculate pair potentials in the unit cell. The above Hamiltonian is diagonalized by a Bogoliubov transformation[45,46] given by

$$C_{j\uparrow}^\dagger(k_y)=\sum_\nu \gamma_\nu^\dagger(k_y)\mathcal{U}_{j,\nu}^*,\quad C_{i\downarrow}(-k_y)=\sum_\nu \gamma_\nu^\dagger(k_y)\mathcal{U}_{N_L+i,\nu}^*,$$

$$C_{j\uparrow}(k_y)=\sum_\nu \mathcal{U}_{j,\nu}\gamma_\nu(k_y),\quad C_{i\downarrow}^\dagger(-k_y)=\sum_\nu \mathcal{U}_{N_L+i,\nu}\gamma_\nu(k_y), \tag{16}$$

where ν is the index which specifies the eigenstates. Then the mean-field Hamiltonian described in Eq. (9) is rewritten as

$$\mathcal{H}_{\rm MF}=\sum_{k_y,\nu} E_\nu(k_y)\,\gamma_\nu^\dagger(k_y)\,\gamma_\nu(k_y), \tag{17}$$

where the operator $\gamma_\nu(k_y)$ satisfies the anticommutation relations

$$\{\gamma_\alpha^\dagger(k_y),\gamma_\beta(k_y')\}=\delta_{\alpha\beta}\delta_{k_yk_y'},$$
$$\{\gamma_\alpha^\dagger(k_y),\gamma_\beta^\dagger(k_y')\}=\{\gamma_\alpha(k_y),\gamma_\beta(k_y')\}=0. \tag{18}$$

The spatial dependence of the pair potential is determined self-consistently as

$$\begin{aligned}\Delta_{j,j\pm m,y}(m)&=\frac{3}{4}J_{\rm eff}\sum_{k_y,\eta,\nu}\mathcal{U}_{j\pm m,\eta}\mathcal{U}_{N_L+j,\nu}^*\langle\gamma_\eta(k_y)\,\gamma_\nu^\dagger(k_y)\rangle e^{\pm ik_ya}\\&=\frac{3}{4}J_{\rm eff}\sum_{k_y,\nu}\mathcal{U}_{j\pm m,\nu}\mathcal{U}_{N_L+j,\nu}^*\{1-f[E_\nu(k_y)]\}e^{\pm ik_ya},\end{aligned} \tag{19}$$

$$\Delta_{j,j\pm1,x}(m)=\frac{3}{4}J_{\rm eff}\sum_{k_y,\nu}\mathcal{U}_{j\pm1,\nu}\mathcal{U}_{N_L+j,\nu}^*\{1-f[E_\nu(k_y)]\}, \tag{20}$$

where $f[E_\nu(k_y)]$ denotes the Fermi distribution function:

$$f[E_\nu(k_y)]=\frac{1}{\exp(E_\nu(k_y)/k_BT)+1}. \tag{21}$$

We solve the effective Hamiltonian, Eq. (9), by numerical diagonalization and carry out an iteration until the pair potentials $\Delta_{ij,x}(m)$ and $\Delta_{ij,y}(m)$ satisfy the self-consistency conditions, Eqs. (19) and (20). The temperature is fixed at $T/t=10^{-7}$. Using the pair potential determined self-consistently, we calculate the LDOS at every site. In order to compare our theory with STS experiments, we assume that the scanning tunnel microscope (STM) tip is metallic with a

flat density of states and that the tunneling probability is finite only for the nearest site from the tip. The LDOS at the ith site is given by[47]

$$\rho_i \sim \int_{-\infty}^{\infty} d\omega\, \rho_i(\omega) \mathrm{sech}^2\left(\frac{\omega - E}{2k_B T}\right), \tag{22}$$

with

$$\rho_i(\omega) = -\frac{2}{\pi} \mathrm{Im} \sum_k G_i^R(k_y, \omega)$$

$$= 2 \sum_k \sum_\nu |\mathcal{U}_{i,\nu}|^2 \delta\{\omega - E_\nu(k_y)\}, \tag{23}$$

where $G_i^R(k_y, \omega)$ is the Fourier component of the retarded Green's function with energy ω. In the actual STM experiments, since the tunneling probability between the tip and surface is small, the tunneling conductance spectrum converges to the normalized LDOS

$$\overline{\rho}(E) = \frac{\int_{-\infty}^{\infty} d\omega\, \rho_{i,S}(\omega) \mathrm{sech}^2\left(\frac{\omega - E}{2k_B T}\right)}{\int_{-\infty}^{\infty} d\omega\, \rho_N(\omega) \mathrm{sech}^2\left(\frac{\omega - 2\Delta_0}{2k_B T}\right)}, \tag{24}$$

at low temperatures,[18] where $\rho_{i,S}(\omega)$ denotes the LDOS in the superconducting state and $\rho_N(\omega)$ denotes the LDOS in the normal state. In this paper, $\rho_N(\omega)$ is obtained from the LDOS at the $[(N_L - 1)/2]$th site far away from the boundary.

III. RESULTS OF NUMERICAL CALCULATIONS

In this section, we study the local density of states and the spatial dependence of the pair potential for various types of surface geometry shown in Fig. 2. To avoid fictitious oscillation of the LDOS due to the small number in the sum of k_y, we have applied a higher temperature $T/t = 5.0 \times 10^{-3}$ for the LDOS than that used in the self-consistent equation. However, this choice of T does not alter the results. First, the hole doping dependence of the superconducting pair potential $\Delta_{\mathrm{SC}}/t = g_t \Delta_0$ (Ref. 40) without the boundary is shown in Fig. 3. The pair potential Δ_{SC}/t is suppressed at the low-doping region. As the doping rate increases, the difference between the four cases becomes clear.

A. Flat (100) surface ($m = 0$)

First, we discuss the case of a flat (100) surface, i.e., the $m = 0$ case shown in Fig. 2(a). Since the pair potentials are complex, we show in Fig. 4(a) their real and imaginary parts:

$$\Delta_{R,j,x}(m) \equiv \mathrm{Re}[\Delta_{j+1,j,x}(m)]/\Delta_0,$$
$$\Delta_{I,j,x}(m) \equiv \mathrm{Im}[\Delta_{j+1,j,x}(m)]/\Delta_0, \tag{25}$$

$$\Delta_{R,j,y}(m) \equiv \mathrm{Re}[\Delta_{j+m,j,y}(m)]/\Delta_0,$$
$$\Delta_{I,j,y}(m) \equiv \mathrm{Im}[\Delta_{j+m,j,y}(m)]/\Delta_0, \tag{26}$$

as a function of the site j. Figure 4(a) is the result for the YBCO-type model with $\delta = 0.05$. It is readily seen that there is no imaginary part, which means that the time-reversal symmetry is not broken in the (100) surface. This situation does not change for any Fermi surface we studied. The real part of the pair potential $\Delta_{R,j,x(y)}(0)$ approaches 1 and -1 in the middle of the superconductor which corresponds to the bulk d-wave state. Near the surface, the s-wave component is mixed since translational symmetry is broken. The calculated LDOS at the surface site of the (100) surface is shown in Fig.

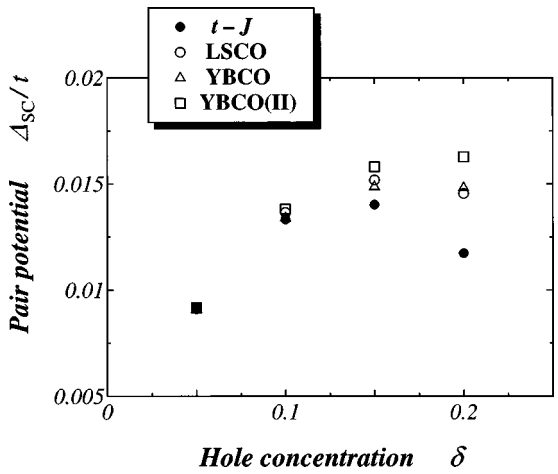

FIG. 3. The hole concentration dependence of the initial value of the bulk superconducting pair potential Δ_{SC}/t within the Gutzwiller approximation for four types of parameters ($J/t = 0.25$).

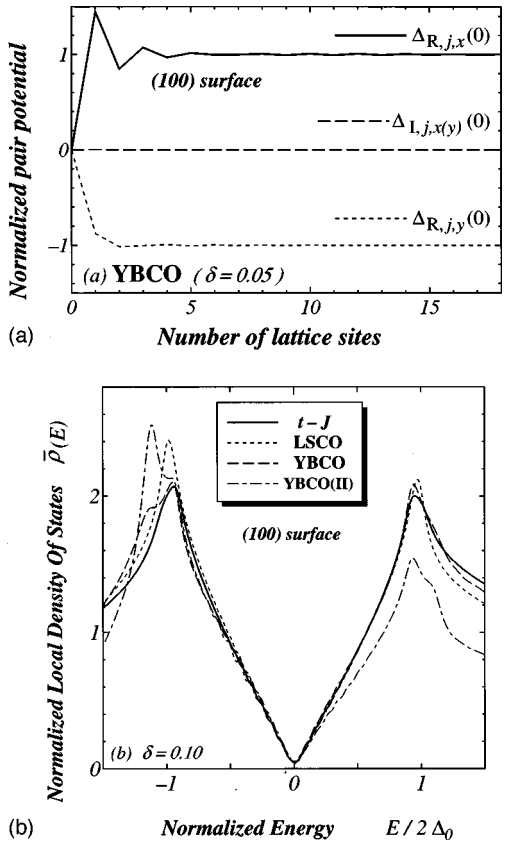

FIG. 4. (a) Spatial dependence of the pair potential $\Delta_{R,j,x(y)}(0)$ and $\Delta_{I,j,x(y)(0)}$ on the (100) surface ($N_L = 401$) for a YBCO-type model ($\delta = 0.05$) and (b) normalized local density of states at the topmost site of the surface for $\delta = 0.10$ and four choices of the Fermi surface.

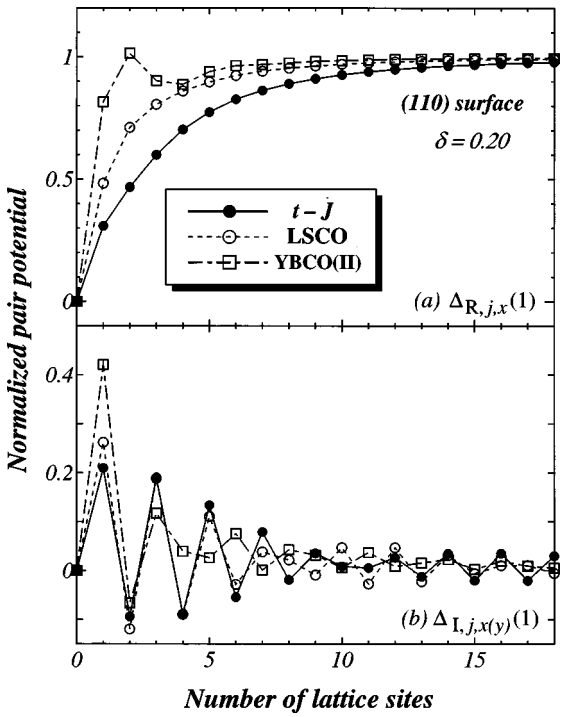

FIG. 5. Spatial dependence of the pair potential (a) $\Delta_{R,j,x(y)}(1)$ and (b) $\Delta_{I,j,x(y)}(1)$ on the (110) surface ($N_L=401$) for a doping rate $\delta=0.20$.

4(b) for a doping rate $\delta=0.10$ and four choices of Fermi surface. Since the quasiparticles do not feel the sign change of the pair potential at the (100) surface,[8,9] the zero-energy peak (ZEP) does not appear.

B. Flat (110) surface ($m=1$)

Next, we study the case of a flat (110) surface, the $m=1$ case. Figure 5 shows the obtained pair potential for the three parameters for t-J model, LSCO type, and YBCO (II) type with $\delta=0.20$. For this (110) surface, we find that the real part of the obtained pair potential always satisfies a relation $\Delta_{R,j,x}(1)=-\Delta_{R,j,y}(1)$. Simultaneously, the imaginary part has a relation $\Delta_{I,j,x}(1)=\Delta_{I,j,y}(1)$. Thus the d-wave component of the pair potential is real and the extended s-wave component is pure imaginary. The latter is induced near the surface as shown in Fig. 5(b). The quantity $\Delta_{R,j,x}(1)$ is suppressed near the surface and increases monotonically toward the middle of the lattice for the t-J and LSCO-type models. These behaviors are consistent with those obtained in the quasiclassical theory.[48] However, the atomic-scale spatial oscillation of the $\Delta_{I,j,x}(1)$ is completely neglected in the quasiclassical approximation. On the other hand, $\Delta_{R,j,x}(1)$ for the YBCO (II)-type model has a complex spatial dependence for $\delta=0.20$. Although the reason for this complex behavior is not clear, there is an apparent tendency that the suppression of the d-wave component in the vicinity of the (110) surface is the largest for the t-J model and the smallest for the YBCO (II) model. The LSCO-type model is intermediate between the former and latter cases. Correspondingly, the amplitude of the induced extended s-wave component is the largest for the YBCO (II) model and the smallest for the t-J model near the surface, as is observed in

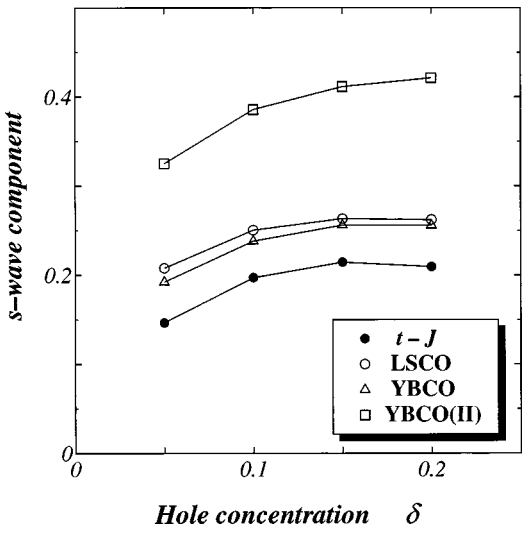

FIG. 6. The doping dependence of the induced s-wave component relative to the bulk d-wave component at the (110) surface site.

Fig. 5(b). However, the s-wave component extends into the middle of the lattice for the t-J model, because the suppression of the d-wave component also does. These results mean that the difference of shape of the Fermi surface leads to quite different features of the spatial dependence of the pair potentials.

We focus on the magnitude of the induced s-wave component. For a typical value of the induced s-wave component, we use $\Delta_{I,j,x}(1)$ at the second site ($j=1$) from the surface. Its doping dependence is shown in Fig. 6 for the four cases we studied. The magnitude of the induced s-wave component depends on the shape of the Fermi surface, but it is enhanced for all the cases as the hole concentration increases. The s-wave component for YBCO (II) is large, but if we use the Fermi surface, YBCO, the induced s-wave component is half compared with that in YBCO (II). This is the main difference between YBCO and YBCO (II). We will

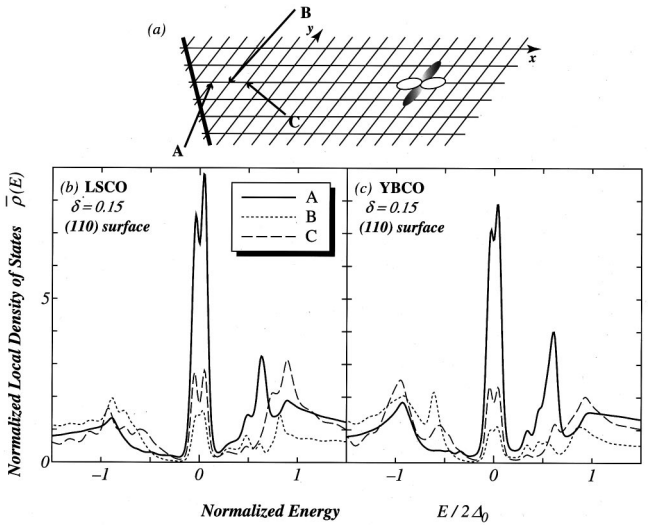

FIG. 7. (a) Schematic illustration of a flat (110) surface and the site dependence of the normalized local density of states with (b) LSCO- and (c) YBCO-type parameters for $\delta=0.15$. The sites A, B, and C are indicated in (a).

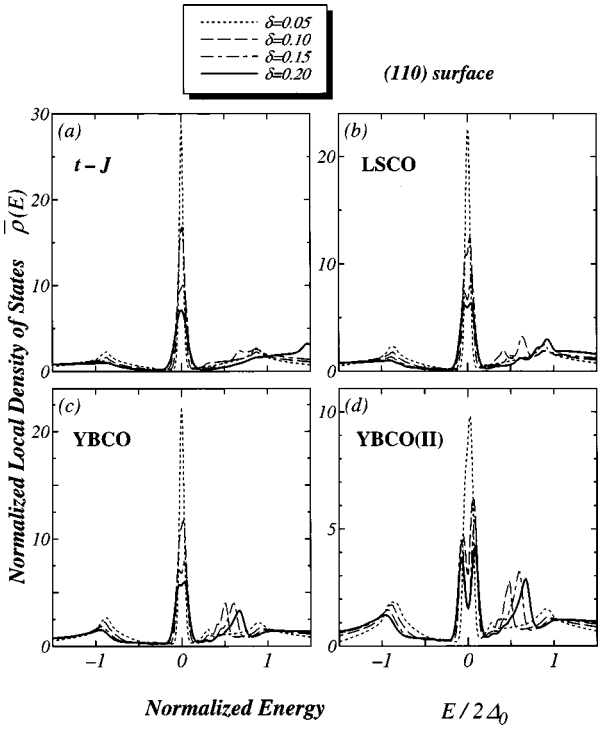

FIG. 8. The doping dependence of the normalized local density of states at the topmost site of a flat (110) surface for four types of parameters for several doping rates.

return to this point shortly. Figures 7(b) and 7(c) show the calculated LDOS for various sites in LSCO- and YBCO-type models, respectively. Apparently, there is a ZBCP and also it has a splitting. In a specularly reflecting (110) surface, a ZES is created because the injected and reflected quasiparticles at the surface feel the sign change of the $d_{x^2-y^2}$-wave pair potential. If the pure imaginary *s*-wave component is induced near the surface, it blocks the motion of quasiparticles near the (110) surface and as a result the bound-state level shifts from zero. This leads to the splitting of the ZBCP. Since the amplitude of the induced *s*-wave component is similar for LSCO and YBCO (Fig. 6), the splitting of the ZBCP is also of the same order for both cases.

The splitting is also obtained in the quasiclassical approximation.[11,26] A remarkable difference between the present results and those based on the quasiclassical theory is seen in the oscillatory behaviors of the LDOS.[10] The ZEP is the largest at site *A*, but it is relatively small at site *B*. Then at site *C*, the ZEP is again enhanced. This oscillation can be regarded as the Friedel oscillation, the period of which is the inverse of the Fermi momentum.

The doping dependence of the LDOS at site *A* is shown in Fig. 8 for the four cases we studied. Comparing with the amplitude of the *s*-wave component shown in Fig. 6, we can easily see that the splitting for each case is roughly proportional to the *s*-wave amplitude. Again, the doping dependences for LSCO and YBCO types are quite similar because the *s*-wave component is similar for both cases. For all cases, the splitting is small for the low doping rate $\delta=0.05$, so that the LDOS have a ZEP. On the other hand, for the high doping rate, the splitting becomes larger. This is because the bulk *d*-wave pair potential is reduced in magnitude with the increase of δ, while the induced *s*-wave component is insensitive to the change of δ.

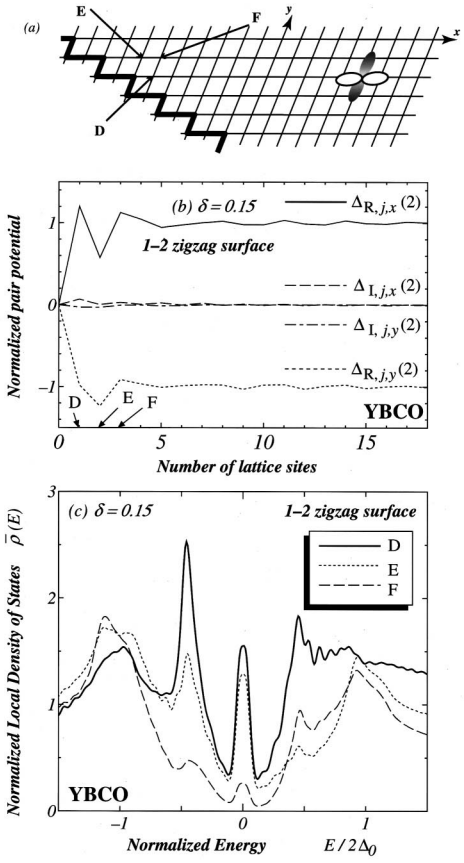

FIG. 9. (a) Schematic illustration of a 1×2 zigzag surface, (b) spatial dependence of the pair potential $\Delta_{R,j,x(y)}(2)$ and $\Delta_{I,j,x(y)}(2)$ on the zigzag surface ($N_L=401$), and (c) the site dependence of the normalized local density of states with YBCO-type ($\delta=0.15$) parameters. The sites *D*, *E*, and *F* are indicated in (a).

Here let us remark on the big difference between YBCO- and YBCO (II)-type models. Although the shapes of the Fermi surface resemble each other, the LDOS near the surface has an obvious difference. This is because the magnitude of the *s*-wave component has a big difference as shown in Fig. 6. Recently, experimental observations of the peak splitting have been reported in the tunneling spectroscopy of high-T_c superconductors.[20,27] Experimentally, the explicit splitting of the ZEP like that of the YBCO (II)-type model is not reported.[20,27] Therefore, we suggest that the YBCO-type model is much more plausible than that of the YBCO (II) type.

C. 1×2 zigzag surface ($m=2$)

In this subsection, we discuss the case of a 1×2 zigzag surface shown in Fig. 9(a). The obtained pair potential is shown in Fig. 9(b), which has a complex spatial dependence as compared to those of (100) and (110) surfaces. The real part of the pair potential $\Delta_{R,j,x(y)}(2)$ has an oscillation near the surface, which cannot be interpreted as a simple *d*-wave component. Since the rotational symmetry is broken, the symmetry other than *d* wave is mixed. We studied the ideal *t-J* model in the previous paper.[36] For that model, the imaginary part $\Delta_{I,j,x(y)}(2)$ is not induced for a 1×2 zigzag surface. However, by adding the next-or third-neighbor transfer

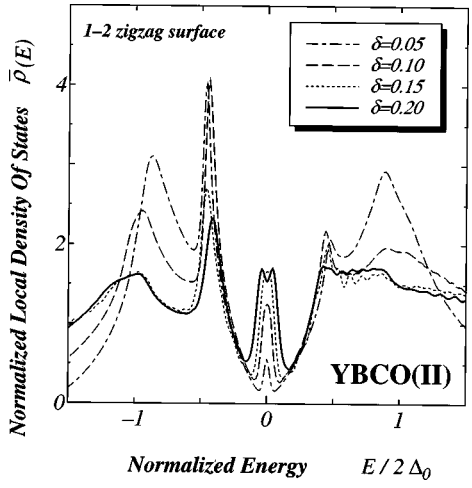

FIG. 10. The doping dependence of the normalized local density of states at the topmost site of a 1×2 zigzag surface for YBCO (II)-type parameter.

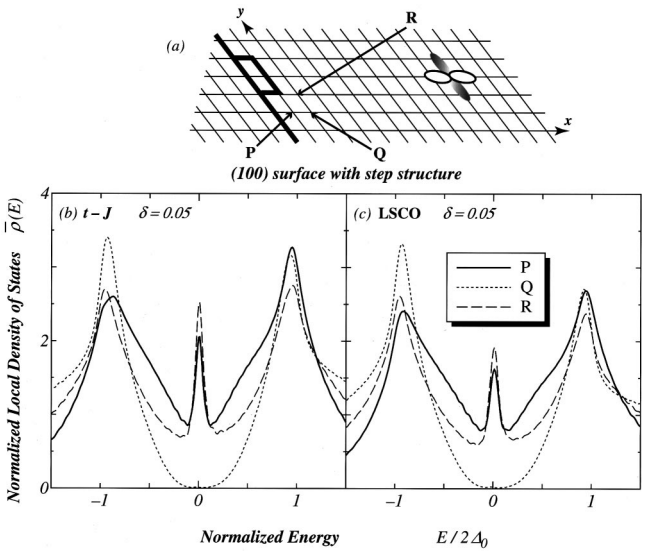

FIG. 11. (a) Schematic illustration of a (100) surface with 1×2 step structure and the site dependence of the normalized local density of states with the (b) t-J model and (c) LSCO-type parameters for $\delta=0.05$. The sites P, Q, and R are indicated in (a).

to the t-J model, the quantity $\Delta_{I,j,x(y)}(2)$ is induced as shown in Fig. 9(b). Furthermore, we find that the magnitude of $\Delta_{I,j,x(y)}(2)$ is enhanced with the increase of the doping concentration.

The complex spatial dependences of the pair potential reflect on the LDOS as an anomalous structure with many dips and peaks as shown in Fig. 9(c). Apart from these anomalous structures, the LDOS has the ZEP at every site near the surface. This is in contrast with our previous results[36] for the ideal t-J model, where the ZES's are not formed near half filling. The reason we considered is as follows. The wave function of the ZES spatially oscillates with the period of the inverse of the Fermi momentum (Friedel oscillation). In the low-doping region, since the Fermi surface is nearly square, the period of the oscillation of the wave function is roughly coincident with $2a$. Consequently, the node and antinode appear alternatively. However, for the 1×2 zigzag structure, the phases of the node and antinode do not coincide. This is the origin of the disappearance of the ZEP for the t-J model. This disappearance can be regarded as an interference effect of the standing wave, which cannot be explained by means of the quasiclassical theory. Compared to this ideal t-J model, because of the t' and t'' hopping integral, LSCO-, YBCO-, and YBCO (II)-type models do not have these interference effects.

In Fig. 10, we show the LDOS for the YBCO (II) case for the 1×2 zigzag surface at the site D. In addition to the ZEP, the splitting of the ZEP is found for $\delta=0.20$. Since the magnitude of the imaginary part (s-wave component) for the YBCO (II)-type model is larger than the other cases, splitting can be seen for a larger doping rate when the relative amplitude of $\Delta_{I,j,x(y)}(2)$ becomes larger.

Finally, with the increase of m, e.g., $m=3,4,\ldots,$ the magnitude of the ZEP in the LDOS is reduced as compared to that of the (110) surface, since the system approaches the (100) surface.

D. (100) surface with step structures

In the previous subsection, Sec. III A, we have shown the absence of the ZES in the LDOS for the (100) surface. Since the appearance of the zero-bias conductance peak in the tunneling spectroscopy is due to the existence of the ZES, we cannot expect the ZBCP for a flat (100) surface. However, in actual experiments, the ZBCP is reported for the (100) surface.[24] One of the possibilities for this inconsistency is the atomic-scale roughness of the surface which inevitably exists in actual samples.[24] To clarify this point, we calculate the LDOS for a (100) surface with defects as shown in Fig. 11. For this geometry, we choose a $N_L\times N_L$ unit cell with an open boundary condition in the x direction and Bloch's boundary condition in the y direction as in Eq. (8), with $N_L=39$ and $N_y=10$. At the position of the step, $t_{\mathbf{ij}}$, $\xi_{\mathbf{ij}}$, and $\Delta_{\mathbf{ij}}$, are set to be zero. We choose a higher temperature $T/t=8.0\times10^{-3}$ than that used in the above subsections, since the numerical diagonalization takes a longer time in this case. However, this choice of temperature T does not alter the results.

We find that the imaginary part of the pair potential is not induced for four types of parameters. The absence of an imaginary part of the pair potential is similar to that in the case around a single impurity.[35] The LDOS in the t-J and LSCO-type models is shown in Figs. 11(b) and 11(c), respectively. Since the imaginary part is not induced, there is no splitting of the ZEP. The ZEP shows up at corner sites P and R near the 1×2 step structure, and these features are consistent with those of previous results based on the extended Hubbard model.[25] The origin of the ZEP is due to the sign change of the pair potentials felt by quasiparticles at the corner sites. The line shapes of the LDOS are different from those near the (110) surface (see Figs. 7 and 8) and are rather similar to those around the single impurity.[35]

IV. SUMMARY

In this paper, we investigated the local density of states near the surface based on the extended t-J model within the Gutzwiller approximation, where several material parameters

are chosen to reproduce the actual Fermi surface of high-T_c superconductors. In the present calculation, the nonlocal feature of the pair potential and the atomic-scale geometry of the surface are explicitly taken into account. Various features of the LDOS are obtained depending on the shape of the Fermi surface and the geometries of the surfaces. Our main results in this paper are summarized as follows.

(i) The LDOS has no ZEP near the flat (100) surface.

(ii) Near the (110) surface, the LDOS has a ZEP and its splitting depending on the magnitude of the induced *s*-wave component. As the doping increases, the splitting becomes larger for any case. The present result serves as the microscopic basis for spontaneous time-reversal symmetry breaking where the *s*-wave component of the pair potential is induced as the imaginary part near the surface. The amplitude of the induced *s*-wave component near the surface is the largest for YBCO (II) and the smallest for the *t*-*J* model. Those for LSCO and YBCO are in between and almost half of that for YBCO (II). Comparing to the recent tunneling experiments of YBCO, the material parameters used in the YBCO-type model are much more reasonable than those in the YBCO (II)-type model.

(iii) For the 1×2 zigzag surface, our results are different from those of the ideal *t*-*J* model where the ZEP is absent. The appearance of the ZEP depends on the doping concentration.

(iv) For the (100) surface with defects, there is the case of the formation of the ZES. This is due to the sign change of the pair potential felt by the quasiparticle due to the atomic-scale roughness.

Recently, since the experimental situation is greatly improved,[24] we can reveal the microscopic parameters of high-T_c superconductors through a detailed comparison of the present results with experimental data by STS.

ACKNOWLEDGMENTS

This work was supported by the Core Research for Evolutional Science and Technology (CREST) of the Japan Science and Technology Corporation (JST). The computational aspect of this work has been performed at the facilities of the Supercomputer Center, Institute for Solid State Physics, University of Tokyo and the Computer Center, Institute for Molecular Science, Okazaki National Research Institute.

[1] D. J. Scalapino, Phys. Rep. **250**, 329 (1995).
[2] M. Sigrist and T. M. Rice, J. Phys. Soc. Jpn. **61**, 4283 (1992); Rev. Mod. Phys. **67**, 503 (1995).
[3] D. A. Wollman, D. J. Van Harlingen, W. C. Lee, D. M. Ginsberg, and A. J. Leggett, Phys. Rev. Lett. **71**, 2134 (1993); D. J. Van Harlingen, Rev. Mod. Phys. **67**, 515 (1995).
[4] I. Iguchi and Z. Wen, Phys. Rev. B **49**, 12 388 (1994).
[5] C. C. Tsuei, J. R. Kirtley, C. C. Chi, L. S. Yu-jahnes, A. Gupta, T. Shaw, J. Z. Sun, and M. B. Ketchen, Phys. Rev. Lett. **73**, 593 (1994).
[6] Y. Tanaka, Phys. Rev. Lett. **72**, 3871 (1994).
[7] A. Mathai, Y. Gim, R. C. Black, A. Amar, and F. C. Wellstood, Phys. Rev. Lett. **74**, 4523 (1995).
[8] C. R. Hu, Phys. Rev. Lett. **72**, 1526 (1994).
[9] Y. Tanaka and S. Kashiwaya, Phys. Rev. Lett. **74**, 3451 (1995); Phys. Rev. B **53**, 9371 (1996).
[10] M. Matsumoto and H. Shiba, J. Phys. Soc. Jpn. **64**, 1703 (1995).
[11] M. Fogelström, D. Rainer, and J. A. Sauls, Phys. Rev. Lett. **79**, 281 (1997).
[12] Yu. S. Barash, A. A. Svidzinsky, and H. Burkhardt, Phys. Rev. B **55**, 15 282 (1997).
[13] J. Geerk, X. X. Xi, and G. Linker, Z. Phys. B **73**, 329 (1988).
[14] I. Iguchi, Physica C **185-196**, 241 (1991).
[15] T. Walsh, Int. J. Mod. Phys. A **6**, 125 (1992).
[16] S. Kashiwaya, M. Koyanagi, M. Matsuda, and K. Kajimura, Physica B **194-196**, 2119 (1994).
[17] S. Kashiwaya, Y. Tanaka, M. Koyanagi, H. Takashima, and K. Kajimura, Phys. Rev. B **51**, 1350 (1995).
[18] S. Kashiwaya, Y. Tanaka, M. Koyanagi, and K. Kajimura, Phys. Rev. B **53**, 2667 (1996).
[19] L. Alff, H. Takashima, S. Kashiwaya, N. Terada, H. Ihara, Y. Tanaka, M. Koyanagi, and K. Kajimura, Phys. Rev. B **55**, 14 757 (1997).
[20] M. Covington, M. Aprili, L. H. Greene, F. Xu, and C. A. Mirkin, Phys. Rev. Lett. **79**, 277 (1997).
[21] S. Sinha and K.-W. Ng, Phys. Rev. Lett. **80**, 1296 (1998).
[22] M. Taira, M. Suzuki, X.-G. Zheng, and T. Hoshino, J. Phys. Soc. Jpn. **67**, 1732 (1998).
[23] J. Y. T. Wei, N.-C. Yeh, D. F. Garrigus, and M. Strasik, Phys. Rev. Lett. **81**, 2542 (1998).
[24] S. Ueno, S. Kashiwaya, N. Terada, K. Kajimura, M. Koyanagi, and Y. Tanaka, J. Phys. Chem. Solids **59**, 2081 (1998).
[25] Y. Tanuma, Y. Tanaka, M. Yamashiro, and S. Kashiwaya, Phys. Rev. B **57**, 7997 (1998).
[26] M. Matsumoto and H. Shiba, J. Phys. Soc. Jpn. **65**, 3384 (1995); **65**, 4867 (1995).
[27] S. Kashiwaya, Y. Tanaka, N. Terada, M. Koyanagi, S. Ueno, L. Alff, H. Takashima, Y. Tanuma, and K. Kajimura, J. Phys. Chem. Solids **59**, 2034 (1998).
[28] F. C. Zhang and T. M. Rice, Phys. Rev. B **37**, 3759 (1988).
[29] M. Ogata, M. Luchini, S. Sorella, and F. Assad, Phys. Rev. Lett. **66**, 2388 (1991).
[30] W. O. Putikka, M. U. Luchini, and T. M. Rice, Phys. Rev. Lett. **68**, 538 (1992).
[31] E. Dagotto and J. Riera, Phys. Rev. Lett. **70**, 682 (1993).
[32] E. Daggoto, Rev. Mod. Phys. **66**, 763 (1994).
[33] H. Yokoyama and M. Ogata, J. Phys. Soc. Jpn. **65**, 3615 (1996).
[34] A. Himeda, M. Ogata, Y. Tanaka, and S. Kashiwaya, J. Phys. Soc. Jpn. **66**, 3367 (1997).
[35] H. Tsuchiura, Y. Tanaka, M. Ogata, and S. Kashiwaya, J. Phys. Soc. Jpn. **67**, 2510 (1999).
[36] Y. Tanuma, Y. Tanaka, M. Ogata, and S. Kashiwaya, J. Phys. Soc. Jpn. **67**, 1118 (1998).
[37] K. Kuboki and M. Sigrist, J. Phys. Soc. Jpn. **67**, 2873 (1998).
[38] C. Honerkamp and M. Sigrist, Physica C **317–318**, 489 (1999).
[39] Jian-Xin Zhu, B. Friedman, and C. S. Ting, Phys. Rev. B **59**, 3353 (1999).
[40] F. C. Zhang, C. Gross, T. M. Rice, and H. Shiba, Supercond. Sci. Technol. **1**, 36 (1988).

[41] T. Tanamoto, H. Kohno, and H. Fukuyama, J. Phys. Soc. Jpn. **61**, 1886 (1992).
[42] T. Tanamoto, H. Kohno, and H. Fukuyama, J. Phys. Soc. Jpn. **62**, 717 (1993).
[43] T. Tanamoto, H. Kohno, and H. Fukuyama, J. Phys. Soc. Jpn. **62**, 1455 (1993).
[44] M. Ogata, J. Phys. Soc. Jpn. **66**, 3375 (1997).
[45] M. Tachiki, S. Takahashi, F. Steglich, and H. Adrian, Z. Phys. B **80**, 161 (1990).
[46] O. Sato, Y. Tanaka, and A. Hasegawa, J. Phys. Soc. Jpn. **61**, 2640 (1992).
[47] M. Tinkham, *Introduction to Superconductivity* (McGraw-Hill, New York, 1975).
[48] Y. Nagato and K. Nagai, Phys. Rev. B **51**, 16 254 (1995).